LSTM-Based Hybrid Modeling Approach for Control Application of Evaporator Involving Phase Transition

Jisung Byun * **Hyein Jung** * **Jong Min Lee** *†

* *Department of Chemical & Biological Engineering, Seoul National University, Seoul, Korea (e-mail: jongmin@snu.ac.kr).*

Abstract: Heat exchangers in vapor compression cycles (VCCs) typically involve phase transitions of the internal refrigerant. While numerous studies have focused on modeling these systems, existing techniques require high computational burden or model switching depending on the refrigerant phase at the heat exchanger outlet. These kinds of problems make each model less suitable for control applications. To overcome these challenges, this study proposes a hybrid model that combines conventional modeling methods with data-driven time series analysis to obtain unified model of heat exchanger with refrigerant phase transition, especially the evaporator in the VCC. The proposed model is fundamentally based on the moving boundary (MB) method, and integrates long short-term memory (LSTM) networks to predict unknown parameters arising from the phase transition. The proposed hybrid model shows high accuracy with the Simulink-Simscape simulation result, and yields higher accuracy compared to a fully data-driven LSTM black-box model, which is another approach to make an unified model. This hybrid approach creates a model that improves accuracy compared to the black-box model and eliminates the need for model switching, ultimately facilitating the design of advanced control.

Keywords: Dynamic modelling and simulation for control and operation, Modeling and identification, Artificial intelligence and machine learning

1. INTRODUCTION

Heat exchangers are fundamental equipment in a wide range of applications, including chemical processes, air conditioning, and power generation. Especially in vapor compression cycles (VCCs), commonly employed for liquefaction and air conditioning, heat exchangers such as evaporators and condensers are significant due to their capability of achieving the desired temperature. Heat exchangers can reduce the electric work requirement by adjusting the temperature gap between fluids, i.e., refrigerant and utility stream. As a result, developing an accurate model of the heat exchanger is essential for predicting its performance and ensuring its efficient operation.

Heat exchangers in VCCs are typically coupled with compression and expansion devices, leading to phase transitions of the working fluid to maintain stable operation. To model these heat exchangers, both the finite volume (FV) method and the moving boundary (MB) method are widely used (Rasmussen, 2012), and a schematic diagram illustrating those methods is shown in Fig 1. The FV method discretizes the heat exchanger into multiple small control volumes, allowing for detailed spatial resolution, but this results in increased computational load as the number of control volumes rises. In contrast, the MB method partitions the heat exchanger based on time-varying phase boundaries. This method is computationally more efficient, requiring fewer variables while still maintaining a high degree of accuracy relative to the FV method (Rasmussen and Shenoy, 2012).

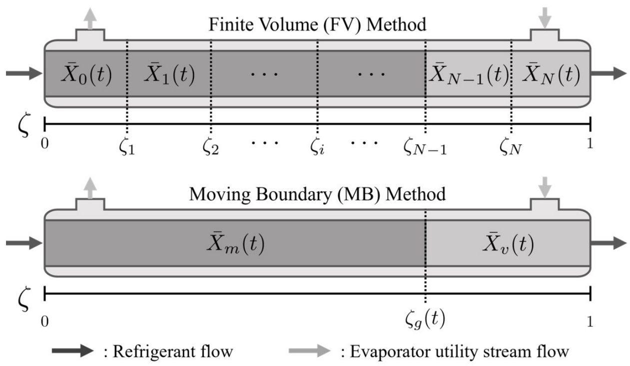

Fig. 1. Two modeling approaches for heat exchanger.

Despite its advantages, the MB method presents challenges in representing the phase transition. One key issue is that the phase boundary may appear or disappear based on the phase of refrigerant at the outlet (Bonilla et al., 2015). In the conventional MB method, the phase variation at the outlet is addressed by constructing separate models for each case and switching between them as needed. However, this approach imposes complexity for model predictive control applications, which should consider the model switching to compute system behavior across multiple time horizons. Moreover, as a lumped parameter model, the MB method simplifies the system through various assumptions, which can introduce discrepancies between the model and the actual system behavior.

In response to these challenges, this study introduces a hybrid modeling approach. Hybrid model combines black-box (data-driven) and white-box (first-principle) models, compensating for the lack of physical insight in the black-box model and the difficulty in capturing the unknown behavior of the system in the white-box model (Sharma and Liu, 2022). We propose a hybrid model that predicts refrigerant phase information using a black-box model based on physical variables such as pressure and specific enthalpy, which is then integrated into a MB model. This approach enhances accuracy by incorporating data-driven insights into unknown parameters while preserving the physical integrity of the heat exchanger behavior through the first-principle model. Moreover, the hybrid model eliminates the need for phase-dependent switching in the MB method, providing a unified model suitable for control applications without requiring model transitions.

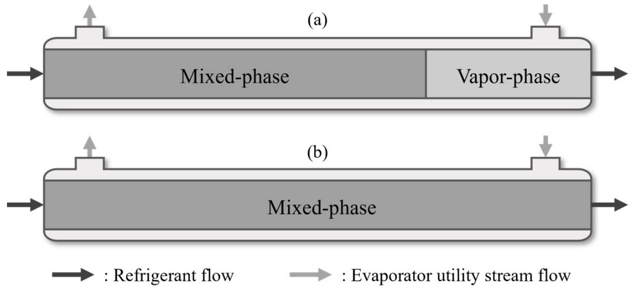

Fig. 2. Two scenarios based on the phase of the refrigerant exiting the evaporator: (a) vapor phase and (b) mixed phase.

This paper focuses on the evaporator in a VCC as the target system. Under normal operating conditions, the refrigerant enters the evaporator from the expansion valve in a mixed phase. However, depending on the heat transfer to the refrigerant within the evaporator, the phase of the refrigerant at the evaporator outlet may vary between mixed phase and vapor phase, as illustrated in Fig. 2. To address the limitations of phase-dependent model switching inherent in the MB method, this study applies hybrid modeling, enabling a unified representation of the evaporator's behavior across all outlet phases.

2. FIRST-PRINCIPLE MODELING OF EVAPORATOR BASED ON MOVING BOUNDARY METHOD

The heat exchanger model is governed by mass and energy balance equations, both of which are originally expressed as partial differential equations (PDEs). The mass balance equation and the energy balance equation are presented in equation (1). A summary of symbols associated with the physical variables is provided in Table A.1.

$$\frac{\partial(\rho V)}{\partial t} + \frac{\partial(\dot{m})}{\partial \zeta} = 0, \quad \frac{\partial(\rho V h - V p)}{dt} + \frac{\partial(\dot{m} h)}{\partial \zeta} = \dot{Q} \quad (1)$$

However, due to the complexity of directly applying PDEs for control purposes, these equations are typically approximated by ordinary differential equations (ODEs). The MB method provides one such approach by dividing the heat exchanger into distinct regions based on phase transition boundaries. In each region, the mass and energy balances are formulated as separate ODEs. This method relies on the Leibniz integration rule, leading to the construction of a model for each control volume ($cv \in \{m, v\}$), as shown in equation (2) and equation (3), representing mass balance and energy balance, respectively. Detailed descriptions on constructing the MB method can be found in studies by Rasmussen and Alleyne (2004), Eldredge et al. (2008), McKinley and Alleyne (2008), and Bonilla et al. (2015).

$$\begin{aligned} V\left[\frac{d}{dt}\int_{\zeta_{cv,in}}^{\zeta_{cv,out}} \rho d\zeta + \rho_{cv,in}\frac{d\zeta_{cv,in}}{dt} - \rho_{cv,out}\frac{d\zeta_{cv,out}}{dt}\right] \\ = \dot{m}_{cv,in} - \dot{m}_{cv,out} \end{aligned} \quad (2)$$

$$\begin{aligned} V\Bigg[\frac{d}{dt}\int_{\zeta_{cv,in}}^{\zeta_{cv,out}} \rho h d\zeta + \rho_{cv,in}h_{cv,in}\frac{d\zeta_{cv,in}}{dt} \\ -\rho_{cv,out}h_{cv,out}\frac{d\zeta_{cv,out}}{dt} - (\zeta_{cv,out} - \zeta_{cv,in})\frac{dp}{dt}\Bigg] \\ = \dot{m}_{cv,in}h_{cv,in} - \dot{m}_{cv,out}h_{cv,out} + \dot{Q}_{cv} \end{aligned} \quad (3)$$

Additionally, the heat transfer rate to the refrigerant is calculated using the effectiveness-NTU method, as shown in equation (4). The effectiveness-NTU method calculates the heat transfer rate as a ratio relative to the maximum possible heat transfer rate (Incropera, 2013). This maximum rate is determined based on the fluid with the lower heat capacity, as the fluid with a lower heat capacity will experience a greater temperature change than the fluid with a higher heat capacity during heat exchange.

$$\begin{aligned} &\dot{Q}_{cv} = \varepsilon_{cv}\dot{Q}_{cv,max} = \varepsilon_{cv}\left(\dot{m}C_p\right)_{min}\left(T_{util,in} - T_{in}\right) \\ &\text{where } \left(\dot{m}C_p\right)_{min} = \min\left\{\left(\dot{m}C_p\right)_{ref}, \left(\dot{m}C_p\right)_{util}\right\} \end{aligned} \quad (4)$$

Detailed elements of the mass matrix and the right-hand side equation of the MB model is represented in Table 1. This model is referred from (Rasmussen and Alleyne, 2004), but is slightly modified by rearranging the mass balance equation leaving only the term $\frac{d\zeta_g}{dt}$ at the left-hand side, and plugging the mass balance equation into energy balance equations.

Solving these expressions yields a final model in an ODE form, structured with a mass matrix in front of the dynamic term ($\dot{x}$), as shown in equation (5). State and input variables, x and u, of the evaporator system are defined as equation (6). Detailed elements inside the mass matrix and the right-hand side equations are provided in Table 1.

$$\begin{aligned} M(x,u)\dot{x} &= \begin{bmatrix} M_{00}(x,u) & M_{01}(x,u) \\ M_{10}(x,u) & M_{11}(x,u) \end{bmatrix}\dot{x} \\ &= \begin{bmatrix} f_0(x,u) \\ f_1(x,u) \end{bmatrix} = f(x,u) \end{aligned} \quad (5)$$

$$\begin{aligned} x &= \left[p \ h_{out}\right]^T \\ u &= \left[\dot{m}_{in} \ \dot{m}_{out} \ h_{in} \ \dot{m}_{util} \ T_{util,in}\right]^T \end{aligned} \quad (6)$$

Table 1. Elements of mass matrix and right-hand side equation inside the evaporator MB model

Mass matrix of equation (5)	
M_{00}	$V\left(a_{00} - a_{02}\dfrac{a_{20}}{a_{22}}\right)$
M_{01}	$-V\left(a_{02}\dfrac{a_{21}}{a_{22}}\right)$
M_{10}	$V\left(a_{10} - a_{12}\dfrac{a_{20}}{a_{22}}\right)$
M_{11}	$V\left(a_{11} - a_{12}\dfrac{a_{21}}{a_{22}}\right)$
Right-hand side of equation (5)	
f_0	$\dot{m}_{in}\left(h_{in} - h_g\right) + \dot{Q}_m - \dfrac{a_{02}}{a_{22}}\left(\dot{m}_{in} - \dot{m}_{out}\right)$
f_1	$\dot{m}_{out}\left(h_g - h_{out}\right) + \dot{Q}_v - \dfrac{a_{12}}{a_{22}}\left(\dot{m}_{in} - \dot{m}_{out}\right)$
Coefficients	
a_{00}	$\zeta_g\left[(1-\bar{\gamma})\left\{\left(h_f - h_g\right)\dfrac{d\rho_f}{dp} + \rho_f\dfrac{dh_f}{dp}\right\} + \bar{\gamma}\rho_g\dfrac{dh_g}{dp} - 1\right]$
a_{02}	$\rho_f\left(h_f - h_g\right)(1-\bar{\gamma})$
a_{10}	$(1-\zeta_g)\left[\left(\bar{h}_v - h_g\right)\left(\dfrac{\partial\bar{\rho}_v}{\partial p} + \dfrac{1}{2}\dfrac{\partial\bar{\rho}_v}{\partial\bar{h}_v}\dfrac{dh_g}{dp}\right) + \dfrac{\rho_v}{2}\dfrac{dh_g}{dp} - 1\right]$
a_{11}	$(1-\zeta_g)\left[\dfrac{1}{2}\left(\bar{h}_v - h_g\right)\dfrac{\partial\bar{\rho}_v}{\partial\bar{h}_v} + \dfrac{\bar{\rho}_v}{2}\right]$
a_{12}	$\bar{\rho}_v\left(h_g - \bar{h}_v\right)$
a_{20}	$\zeta_g\left(\bar{\gamma}\dfrac{d\rho_g}{dp} + (1-\bar{\gamma})\dfrac{d\rho_f}{dp}\right) + (1-\zeta_g)\left(\dfrac{\partial\bar{\rho}_v}{\partial p} + \dfrac{1}{2}\dfrac{\partial\bar{\rho}_v}{\partial\bar{h}_v}\dfrac{dh_g}{dp}\right)$
a_{21}	$\dfrac{1}{2}\dfrac{\partial\bar{\rho}_v}{\partial\bar{h}_v}(1-\zeta_g)$
a_{22}	$(\rho_g - \bar{\rho}_v) + \left(\rho_f - \rho_g\right)(1-\bar{\gamma})$

This study seeks to model the behavior of the evaporator using a single, unified model without the need for model switching. To achieve this, an MB model is developed with both the mixed phase and vapor phase refrigerant inside the evaporator. However, as the phase transition boundary approaches the evaporator outlet, the original model with both phase region encounters a singularity in the mass matrix, making it challenging to accurately represent scenarios where the refrigerant exits in the mixed phase. To address this limitation, the proposed model requires the estimation of key parameters, such as non-dimensional position of phase boundary (ζ_g), the mean void fraction ($\bar{\gamma}$), and the heat exchange effectiveness factors for the mixed and vapor phases (ε_m, ε_v). The non-dimensional position of phase boundary ranges between 0 and 1, as it represents the actual location of the phase boundary within the evaporator. Moreover, when the refrigerant exits in the vapor phase, the heat exchange effectiveness factors range between 0 and 1, as the heat transfer rate is defined as a positive value. Heat transfer occurs in both the mixed and vapor phase regions, influencing the effectiveness of the process. However, when the refrigerant exits in the mixed phase, these values may deviate from this range to make the model to operate similarly with the actual behavior of the system.

3. HYBRID MODELING OF EVAPORATOR

This study employs a hybrid modeling approach to represent different refrigerant outlet phases in a single heat exchanger model and estimate the parameters for each case. Hybrid modeling integrates a first-principle model with a data-driven model to correct for physical characteristics, biases, or noise that the first-principle model alone cannot capture.

3.1 Long short-term memory (LSTM)

LSTM, a type of recurrent neural network (RNN), incorporates gating mechanisms into the basic RNN structure to mitigate issues such as vanishing gradient (Hochreiter, 1997). LSTM is particularly effective in identifying patterns within time-series data, widely applied as black-box or hybrid models in chemical process modeling.

In this study, LSTM is employed to predict process parameters, with the goal of capturing the dynamic characteristics of parameters associated with phase transition by utilizing both current and historical data. While the MB model inherently assumes that the position of phase boundary varies over time, the proposed hybrid model treats variables related to phase transition as parameters to be estimated. Therefore, the LSTM is integrated as the black-box component of the hybrid model to account for the time-dependency of parameters.

3.2 Configuration of hybrid model

The two most common hybrid model structures are the parallel and serial configurations, as shown in Fig. 3. In the parallel hybrid structure, the machine learning model learns and compensates for the discrepancy between the first-principle model and empirical data. In contrast, the serial hybrid structure estimates unknown parameters or disturbances not captured by the first-principle model and integrates them into the model. Above those hybrid model structures, the serial hybrid structure is commonly used for the unknown parameter estimation (Sansana et al., 2021). Owing to this property, this study employs a serial hybrid model to estimate the unknown parameters of the MB model.

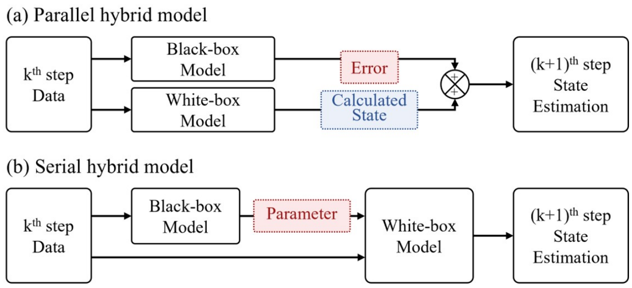

Fig. 3. Serial hybrid modeling structure for evaporator.

Unlike conventional methodologies for estimating system parameters and state variables, such as the Extended Kalman Filter (EKF), serial hybrid models do not assume that parameter values remain fixed after incorporating feedback. Instead, they represent parameters as functions dependent on state and input variables, allowing for a more adaptive and physically consistent modeling approach. By dynamically capturing system behavior rather than relying on real-time feedback , the serial hybrid model provides a more accurate representation of the underlying physics. This enhanced model fidelity enables model-based control to compute more suitable and optimal input variables, ultimately improving system performance and control precision.

3.3 Construction of hybrid model

In this study, the hybrid model combines the MB method, outlined in Section 2, with LSTM for unknown parameter estimation. The overall structure of the proposed hybrid model is illustrated in Fig. 4. In the proposed hybrid model, the LSTM-based black-box component utilizes the data at the current time step and learns the optimal parameters to minimize the discrepancy between the predicted and actual state variable values at the subsequent time step. These optimal parameters are pre-determined in the offline basis by solving an optimization problem with the use of MATLAB's *fmincon* function. Using the current time step data and the parameters obtained from the black-box model, the hybrid model predicts the state variables for the next time step.

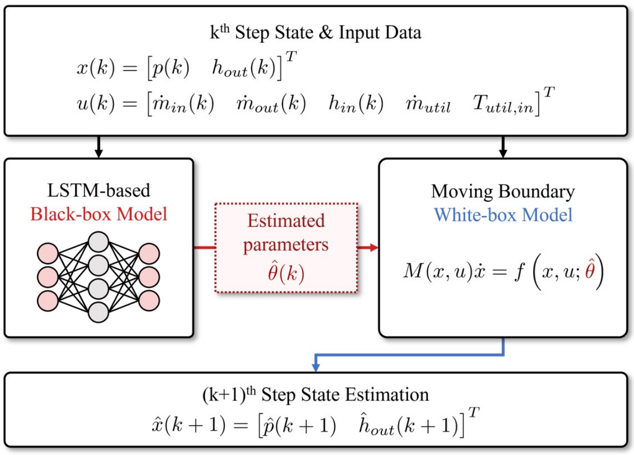

Fig. 4. Serial hybrid modeling structure for evaporator.

To obtain the LSTM-based model, hyperparameters listed in Table 2 were used. All training data were preprocessed through normalization, scaling each value between 0 and 1 based on the minimum and maximum values within the dataset. This process mitigates the impact of scale differences between data variables on the learning performance.

Table 2. Hyperparameters of LSTM model in the proposed hybrid model

Hyperparameter	Value
Layer sequence	LSTM, Dense
Number of nodes	128, 32
Number of lookbacks	30
Batch size	256
Epochs	304/1000
Learning rate	0.013
Dropout ratio	0.1
Loss metric	Mean squared error (MSE)
Optimizer	ADAM
Train:Test:Valid	0.6:0.2:0.2

4. MODEL VALIDATION AND DISCUSSION

4.1 Simulation design of evaporator

This study employs simulation results from MathWorks' Simulink-Simscape to validate the performance of the proposed hybrid model. The block used in the simulation is *Condenser Evaporator (TL-2P)*, and counter flow heat exchanger is assumed. More detailed settings of this block are shown in Table 3. R-1234yf (2,3,3,3-tetrafluoropropene) was used as the refrigerant within the evaporator, while a 50:50 mixture of ethylene glycol and water by volume serves as the hot side utility stream. The input variables for the simulation align with those defined for the MB model in Section 2, but both $\dot{m}_{in}$ and $\dot{m}_{out}$ are set equal to ensure mass balance within the evaporator. To reflect prior knowledge that the refrigerant typically enters the evaporator as a mixed phase after passing through the expansion valve, the input range of the refrigerant's specific enthalpy was set within mixed-phase conditions.

Table 3. Simscape evaporator settings

Configuration	
Flow arrangement	Counter flow
Cross sectional area	0.01 (m^2)
Two-phase Liquid (Refrigerant)	
Number of tubes	10
Tube cross section	Rectangular
Tube length	0.5 (m)
Tube width	0.1 (m)
Tube height	0.005 (m)
Pressure loss coeff.	125
Heat transfer coeff. model	Colburn equation
[a, b, c] in colburn equation — liquid	[0.023, 0.8, 0.33]
[a, b, c] in colburn equation — mixed	[0.280, 0.8, 0.33]
[a, b, c] in colburn equation — vapor	[0.023, 0.8, 0.33]
Fouling factor	0.1 (K·m^2/kW)
Total fin surface area	0 (m^2)
Fin efficiency	0.5
Initial pressure	150 (kPa)
Initial quality	0.5
Thermal Liquid (Utility)	
Number of tubes	10
Tube cross section	Rectangular
Flow geometry	Flow inside one or more tubes
Tube length	0.5 (m)
Tube width	0.1 (m)
Tube height	0.005 (m)
Pressure loss coeff.	125
Heat transfer coeff. model	Colburn equation
$[a, b, c]$ in Colburn equation	[0.0861, 0.8, 0.33]
Fouling factor	0.1 (K·m^2/kW)
Total fin surface area	0 (m^2)
Fin efficiency	0
Initial pressure	101.325 (kPa)
Initial temperature	0 (^{o}C)

The dataset was generated from 100,000 seconds of simulated data in Simulink with a sampling time of 2 seconds. After discarding the first 80 seconds to remove transient effects, the remaining data was chronologically split into training, validation, and test sets in a 0.6:0.2:0.2 ratio for parameter learning. Detailed simulation settings are summarized in Table 4. The overall structure of the simulation and hybrid model construction is illustrated in Fig. 5.

4.2 Model validation results

To assess the performance of the proposed hybrid model, predictions of state variables from the hybrid model were compared against data from Simulink-Simscape simulations. Additionally, to determine whether the integration of the MB model with the LSTM black-box compensates

Table 4. Simulation settings

Refrigerant and Utility			
Refrigerant	R-1234yf (2,3,3,3-tetrafluoropropene)		
Utility stream	Ethylene Glycol:water=50:50 (vol%)		
Input variable bounds			
Variable	Lower	Upper	Unit
$\dot{m}$	0.01	0.05	(kg/s)
h_{in}	210	290	(kJ/kg)
$\dot{m}_{util}$	0.4	1.2	(kg/s)
$T_{util,in}$	-10	10	(^{o}C)
Simulation settings			
Time step	2 (sec)		
Step change	10 (sec)		
Total simulation time	100,000 (sec)		

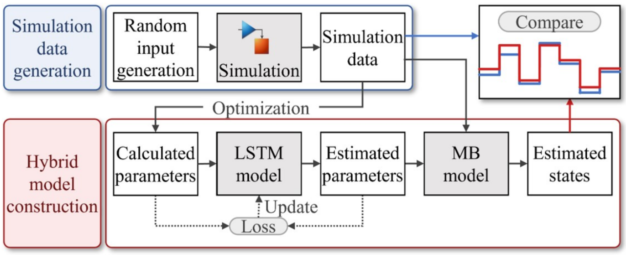

Fig. 5. Overall schematic diagram of simulation and hybrid model construction.

for the limitations of purely data-driven models lacking physical knowledge, we evaluated the model's time series dynamics predictions compared to a black-box model. The hyperparameters used for the black-box model in this validation are set equal to those of the hybrid model.

Fig. 6 presents the results from the proposed hybrid model and the black-box model, along with the Simulink-Simscape simulation data and MB model result. The time domain presented in Fig. 6 is a selected subset from a region within the test set, corresponding to data recorded after 80,016 seconds. This result demonstrates that the proposed hybrid model closely aligns with the results obtained from the Simulink-Simscape simulation. While both the hybrid model and the black-box model capture the overall trends, the hybrid model exhibits reduced bias relative to actual data, leading to improved accuracy.

Table 5 summarizes the mean absolute percentage error (MAPE) values, which quantify the accuracy of the predictions on the test set, as well as the training and one-step computation time of each model. While the MB model which explicitly represents phase change through multiple models demonstrated the highest performance, the hybrid model formulated as a single model achieved comparable accuracy. The black-box model exhibited lower accuracy than both the MB and hybrid models.

Table 5. Test set MAPE and computation time

Model	Hybrid	Black-box	MB
MAPE of p (%)	0.932	4.439	0.860
MAPE of h_{out} (%)	0.475	1.133	0.142
Training time (sec)	1281.64	1790.06	-
One-step computation time (sec/step)	0.00392	0.00160	0.00112

The training time differed by approximately 500 seconds between the hybrid and black-box models, likely due to variations in the number of epochs required to meet the early-stopping criterion. The computation time was approximately 0.001 seconds per step for both the the MB and black-box models, while the hybrid model required around 0.003 seconds per step. Although the hybrid model has a slightly higher computational cost, its computation time remains sufficiently fast for real-time applications, and thus is expected to be suitable for use in control models.

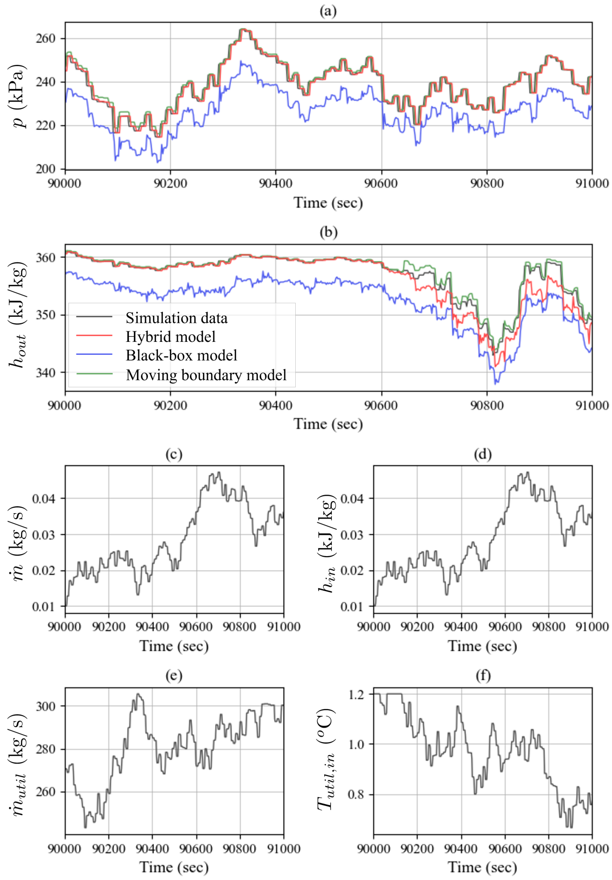

Fig. 6. Comparison of the simulation data, hybrid model estimation, and black-box model estimation, within the test set.

Fig. 7 compares the values of the unknown parameter obtained from a priori optimization on the test set data with those predicted by the LSTM component of the hybrid model. In Fig. 7(a), the operating region encompassed both data points where $\zeta_g = 1$, indicating two-phase refrigerant at the evaporator outlet, and data where $\zeta_g < 1$, representing superheated vapor. While some biases exist between the LSTM-predicted parameters and those derived from direct optimization, the overall trends are well-aligned. Notably, in the latter part of Fig. 7(a), the LSTM model effectively differentiates between mixed and vapor phase outlets. This concludes that the proposed hybrid model can capture the system's behavior with a unified approach, eliminating the need for model switching based on the refrigerant phase at the evaporator outlet.

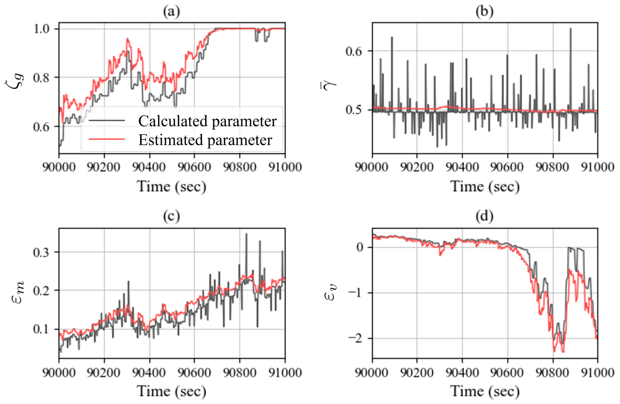

Fig. 7. Comparison of the parameters optimized from the simulation data and estimated from the hybrid model.

5. CONCLUSION

This study introduces a hybrid modeling approach that integrates the MB method with an LSTM model to address challenges in conventional modeling methodologies, particularly those arising from phase transitions in refrigerant exiting the evaporator. The hybrid model employs the LSTM black-box model to predict system parameters associated with phase transitions, which are then incorporated, alongside data from the previous time step, into the MB-based white-box model to predict state variables for the subsequent time step.

The proposed hybrid approach effectively simulates phase transitions at the evaporator outlet using a unified model, eliminating the need for model switching. This addresses a key limitation of traditional MB models, where multiple models must be constructed and switched depending on the evaporator outlet phase, complicating their application in controller design. By improving model accuracy and overcoming the constraints of existing evaporator models, the hybrid model presented here has the potential to enhance the performance in model-based control.

Although this study focuses on the evaporator, the approach can be extended to the condenser and the entire VCC system. Developing a hybrid model for the VCC system would enable more comprehensive implementation and control, accommodating various operational objectives such as cooling and heating. Furthermore, validating the extrapolation performance of the proposed hybrid model could contribute to the development of a more effective control model.

In this context, LSTM was employed as the black-box component for hybrid modeling, but further exploration of alternative time-series analysis techniques is necessary. Deeper investigation is needed to compare methods such as GRU, attention mechanisms, and transformers with LSTM to evaluate their effectiveness in improving hybrid modeling and control performance. Future work will focus on extending the hybrid model to the entire VCC system and evaluating its effectiveness for control by assessing its performance in both interpolation and extrapolation scenarios using various time-series analysis methods.

REFERENCES

Bonilla, J., Dormido, S., and Cellier, F.E. (2015). Switching moving boundary models for two-phase flow evaporators and condensers. *Communications in nonlinear science and numerical simulation*, 20(3), 743–768.

Eldredge, B.D., Rasmussen, B.P., and Alleyne, A.G. (2008). Moving-boundary heat exchanger models with variable outlet phase. *Journal of Dynamic Systems, Measurement, and Control*, 130.

Hochreiter, S. (1997). Long short-term memory. *Neural Computation MIT-Press*.

Incropera, F.P. (2013). Principles of heat and mass transfer.

McKinley, T.L. and Alleyne, A.G. (2008). An advanced nonlinear switched heat exchanger model for vapor compression cycles using the moving-boundary method. *International Journal of refrigeration*, 31(7), 1253–1264.

Rasmussen, B.P. (2012). Dynamic modeling for vapor compression systems—part i: Literature review. *HVAC&R Research*, 18(5), 934–955.

Rasmussen, B.P. and Alleyne, A.G. (2004). Control-oriented modeling of transcritical vapor compression systems. *J. Dyn. Sys., Meas., Control*, 126(1), 54–64.

Rasmussen, B.P. and Shenoy, B. (2012). Dynamic modeling for vapor compression systems—part ii: Simulation tutorial. *HVAC&R Research*, 18(5), 956–973.

Sansana, J., Joswiak, M.N., Castillo, I., Wang, Z., Rendall, R., Chiang, L.H., and Reis, M.S. (2021). Recent trends on hybrid modeling for industry 4.0. *Computers & Chemical Engineering*, 151, 107365.

Sharma, N. and Liu, Y. (2022). A hybrid science-guided machine learning approach for modeling chemical processes: A review. *AIChE Journal*, 68(5), e17609.

Appendix A. NOTATIONS OF THE VARIABLES

The notations employed throughout this paper are summarized in Table A.1. All variables associated with physical properties without subscripts refer to values for the refrigerant (ref). Bar notation of a physical quantity $X(\bar{X})$ represents the arithmetic mean along the control volume.

Table A.1. Elements of mass matrix and right-hand side equation inside the evaporator MB model

Symbols			
C_p	Specific heat	Q	Heat transfer rate
T	Temperature	V	Volume
h	Specific enthalpy	$\dot{m}$	Mass flow rate
p	Pressure	t	Time
γ	Void fraction	ε	Effectiveness factor
ρ	Density	ζ	Phase boundary $\in [0, 1]$
Subscripts			
f	Liquid saturation	g	Vapor saturation
m	Mixed phase	v	Vapor phase
cv	Control volume	in	Inlet flow
out	Outlet flow	$util$	Utility stream